

## Analysis of Mixed-Mode Cracks in a Rubbery Particulate Composite

Timothy C. Miller

Air Force Research Laboratory  
AFRL/PRSM, 10 East Saturn Blvd.  
Edwards Air Force Base, California, USA 93524  
(661) 275-5323 FAX (661) 275-5435

### ABSTRACT

The mixed-mode loading of a rubbery particulate composite is studied experimentally. Linear fracture mechanics concepts are used to determine the initiation of growth, the initial growth direction, and the subsequent growth rate for a range of mode mixities. The fracture toughness locus is determined to be elliptical, with the mode II toughness being lower than its mode I counterpart. The initial growth directions correlate with maximum strain energy density theories. The crack growth rates can be modeled effectively using an equivalent mode I crack.

(keywords: A: particle reinforcement, B: fracture, mixed-mode loading)

### INTRODUCTION

A crack may form in a rubbery particulate composite during manufacture, handling, or storage of a component. Such a crack will be in the mode I loading orientation during this transient state, but will later encounter mixed-mode loading (also called combined loading) when the actual service loads are applied. Mixed-mode loading also is encountered when an intrinsic defect causes a crack to form at an angle to the nominal mode I loading direction.

An early study by Erdogan and Sih used maximum tangential stress theory to predict the initial crack growth angle (also called the kink angle) and the fracture toughness.<sup>1,2</sup> The fracture toughness for mixed-mode loading can be described by two parameters, most often the mode I and mode II fracture toughnesses,  $K_{IC}$  and  $K_{IIC}$ , although magnitude and phase angle are also used. For mixed-mode loading of isotropic materials, an elliptical fracture toughness locus has often been used.<sup>3</sup> Wu analyzed orthotropic materials under combined loading and fit the fracture toughnesses with a similar empirical curve fit.<sup>4,5</sup> Spencer and Barnby generalized the results to anisotropic materials.<sup>5,6</sup> Two-parameter failure loci based on microstructural assumptions were developed by Evans and Hutchinson and by Shih and Suresh.<sup>7,8</sup> Numerous experimental works have confirmed all these empirical curve fits, though few have dealt with rubbery particulate composites.<sup>2-6,9</sup>

Approved for public release; distribution unlimited

For many materials, the fracture locus formed by plotting critical combinations of  $K_{IC}$  and  $K_{IIC}$  will be elliptical due to changes in micromechanisms that cause differences in the toughness as the mixity changes. However, the relationship between the fracture toughness locus and related microstructural phenomena are not well understood.<sup>10</sup> Wu examined micromechanisms in fibrous composites, and Evans and Hutchinson postulated a surface roughness effect to explain increased toughness with mode II loading.<sup>4,7</sup> Researchers have also suggested effects due to nonlinear material properties such as plasticity.<sup>7,8,11</sup> These relationships have merit for some classes of materials (e.g., metals), but may not apply to rubbery particulate composites.

The direction in which the mixed-mode crack will begin to grow has also been studied. Researchers have proposed various criteria to determine the kink angle, or initial crack growth direction.<sup>1,2,5,10</sup> However, these theories may not completely explain the behavior of rubbery particulate composites, which employ a rubbery matrix material to provide structure for the rigid particles. Because of the matrix material, the composite can sustain large deformations. Several different types of embedded particles make up a large volume fraction (70-80%) of the composite.

The actual mixed-mode crack behavior in these composites can be characterized by answering three questions:

1. Under what conditions will a crack start to grow?
2. If the crack grows, what path will it take?
3. At what rate will this growth occur?

The first question addresses conditions for initiation of growth, the second addresses the kink angle, and the third deals with the growth rate. All of these phenomena depend on the mode mixity and are important to the service life prediction. As an example, the initiation of crack growth under different combined loads will depend upon two components of fracture toughness,  $K_{IC}$  and  $K_{IIC}$ . The fracture toughness locus can be determined by a series of experiments. Researchers can then use a numerical method such as the finite element method, along with approximations of the service loads and geometry, to determine the complex stress intensity factor,  $\vec{K} = K_I + iK_{II}$ . This stress intensity factor can be plotted on the failure locus to determine if the given crack will grow.

The kink angle, or initial crack growth direction, is also important, because it determines the crack path during the initial stages of growth. If a defect or other feature (for example, an interface or a free surface) exists

near the crack, growth toward it and the resulting interaction could result in accelerated crack growth and component failure.

The last significant consideration that affects the service life prediction is the crack growth rate. In many instances, the growing crack will grow slowly enough to be noncritical throughout the service life. However, the need to prevent catastrophic fracture requires that the growth rate be quantified before the part can be approved for use. Consequently, more accurate appraisals of the growth rate will result in the ability to use components that were previously questionable.

The current experimental work addresses these issues in a useful and simple manner. The use of a similar procedure for other particulate composite materials will give the investigator the ability to predict the initiation of growth, the initial growth direction, and the subsequent crack growth rate for mixed-mode cracks. This is achieved with linear fracture mechanics concepts. Despite the viscoelastic nature of the rubbery composite, the linear approach provides predictive capability (for a given nominal strain rate) and can be used without a thorough knowledge of the time dependent behavior, which would require more elaborate experimentation and analysis.

#### EXPERIMENTAL PROCEDURE

*Figure 1* shows a typical specimen used here. The cracks are at an angle  $\beta$  to the mode I loading direction. For a crack in an infinite plate of a linear elastic material, in-plane traction boundary conditions results in stress intensity factors given by <sup>12</sup>:

$$\begin{aligned} K_I &= \sigma \sqrt{\pi a} \cos^2 \beta \\ K_{II} &= \sigma \sqrt{\pi a} \sin \beta \cos \beta \end{aligned} \quad (1)$$

Here  $K_I$  and  $K_{II}$  are the mode I and mode II stress intensity factors,  $\sigma$  is the remote nominal stress, and  $a$  is the crack length. This formula applies to an infinite plate with traction boundary conditions. In such a case, the crack orientation,  $\beta$ , is identical to the phase angle of the complex stress intensity factor, defined by  $\Psi$  below:

$$\tilde{K} = K_I + iK_{II} = Ke^{i\Psi} \quad (2)$$

Here the complex stress intensity factor has real and imaginary parts  $K_I$  and  $K_{II}$  but can also be characterized by the magnitude,  $K$ , and phase angle  $\Psi$ . The actual specimens were of finite width and had displacement boundary conditions, but finite element analysis revealed that the phase angles of  $\vec{K}$  for these finite width specimens were also approximately equal to the crack orientation angle  $\beta$ . We tested two specimens for each of five different crack orientations: 0, 15, 30, 45, and 60 degrees.

A displacement controlled testing machine loaded the specimens at a fixed rate of 5.08 mm/min. A special fixture applied uniform vertical displacements to the upper and lower edges of the specimens. During testing, the specimens were videotaped. We synchronized the images with the load-displacement data to determine the time, displacement, and load at which crack growth began. Before crack growth, significant crack tip blunting occurs due to the large deformations that the material can sustain. The actual growth occurs by the damage of material near the crack tip. Under increasing loads, the particles near the crack tip separate from the rubbery matrix, resulting in the nucleation of voids which then coalesce with the macrocrack.

The determination of the boundary conditions at initiation is easily accomplished using the videotape equipment and the testing machine. These boundary conditions (edge displacements in this case) can be applied to a finite element model that uses constitutive properties determined from tensile tests (see *Figure 2* for an example of a mesh). The finite element results include the  $J$  integral, determined here using the domain integral. The  $J$  integral and the magnitude of  $\vec{K}$  are simply related through <sup>13</sup>:

$$J = \frac{K^2}{E'}, \quad E' = E(\text{plane stress}), \quad E' = \frac{E}{1 - \nu^2}(\text{plane strain}) . \quad (3)$$

The phase angle,  $\Psi$ , can be evaluated using the crack flank displacements. The opening and sliding relative displacements of the two faces are determined in the limit as  $r \rightarrow 0$  and related to the phase angle of  $\vec{K}$ . A slightly different method uses the stresses  $\sigma_{yy}$  and  $\sigma_{xy}$  along the positive  $x$  axis. Analysis using these methods revealed that for the plate specimens, the crack orientation angle,  $\beta$ , and the phase angle,  $\Psi$ , are about equal, so that

the phase angle  $\Psi$  was taken to be identical to the crack orientation angle  $\beta$  for the remainder of this work.

However, for determination of the phase angle in an actual structure, the use of crack flank displacements, stresses along the  $x$  axis, or some other method is necessary.

The use of eqn (3) for determining the magnitude of  $\bar{K}$  and the knowledge that  $\beta \cong \Psi$  provide a way to calculate  $\bar{K}$  completely. Using the boundary conditions (determined from the videotape and load-displacement data) at the point of crack growth initiation and incorporating these boundary conditions into the finite element model gives the fracture toughness in terms of  $K_{IC}$  and  $K_{IIC}$ , or, alternatively,  $K_C$  and  $\Psi$ .

Finite element models were used with experimental results to determine the initiation of growth in the various specimens, but the kink angles were determined with experimental data only. *Figure 3* shows a crack in a specimen (the crack orientation angle was  $60^\circ$ ). This picture was taken a short time after crack growth had begun. As the figure shows, trying to define the initial direction of the crack is complicated by the large deformations, and results in ambiguity. These complications are avoided by determining the kink angles from the fracture surfaces of the specimens after final fracture.

As the mesh in *Figure 2* shows, the model is constructed without using a "spider web" near the crack tip. Releasing nodes in front of the crack tip allows for growth, but only in a self similar fashion. A mixed-mode crack does not grow in a self similar manner, however, but instead grows along a curved trajectory for a short time until it orients itself with the mode I direction. A precise analysis of this phenomenon would require a complicated analysis and numerous meshes since the instantaneous crack growth direction cannot be predetermined. An alternative method was used here, and is shown in *Figure 4*. For a given specimen, the projection of the crack profile onto a horizontal plane was measured from videotape images, and was synchronized with the load-displacement data so that the effective crack length and the load were known at different times during the crack growth. Thus the irregularly shaped mixed-mode crack was modeled as a flat mode I crack, which could then be analyzed more easily. This is justified by the tendency of the crack to grow in the mode I direction after a small amount of crack growth has occurred, and is also suggested by the similar curve fits for  $da_{eff}/dt$  versus  $K_I$  data for all the different mixities tested.

An added complication of the crack growth analysis in rubbery composites is the sporadic nature of the crack growth. The crack growth in this highly filled composite takes place by nucleation, growth, and subsequent

coalescence of voids ahead of the crack tip. During this process, the crack growth rate will be uneven, with intermediate periods of blunting and slow growth. Measuring and plotting  $a_{eff}$  versus  $t$  in this situation will give growth rates that cannot be reconciled with any fracture parameters or remote loading conditions. Therefore attempts to relate  $da_{eff}/dt$  to the remote loads through  $K_I$  will give inconsistent results unless the results are smoothed before relating them to crack tip parameters such as  $K_I$ . The investigator can use any of several techniques to smooth the crack size versus time data before derivation of the crack growth rate without influencing the resulting predictions significantly. Techniques such as the secant method, the incremental polynomial method, and the polynomial method have been used in past analyses of mode I cracks. Using this experience as a guide, we have used the polynomial method. The crack growth versus time data for each trial is fitted with a cubic polynomial, which is then differentiated to determine the crack velocity,  $da_{eff}/dt$ .

## RESULTS

Results for initiation of growth as determined from the experimental results are shown in *Figure 5*. The associated curve is an elliptical curve of the form:

$$\left( \frac{K_I}{K_{IC}} \right)^2 + \left( \frac{K_{II}}{K_{IIC}} \right)^2 = 1 \quad . \quad (4)$$

Here the mode I and mode II toughnesses ( $K_{IC}$  and  $K_{IIC}$ , respectively) are regarded as unknown parameters and are found using a least-squares adjustment of the data.<sup>14</sup> Equation (4) is regarded as linear with respect to the fitting parameters  $(1/K_{IC})^2$  and  $(1/K_{IIC})^2$  and these unknowns are found by minimizing the sum of the square of the residuals. Assuming random variations in the toughness measurements, this procedure allows for a determination of  $K_{IIC}$  although specimens experiencing pure mode II conditions are never tested. As the figure shows, the mode II fracture toughness is significantly lower than its mode I counterpart. This suggests that different mechanisms govern fracture as the mode-mixity changes. However, there are no sufficient explanations of this phenomenon that apply to a rubbery particulate composite. Evans and Hutchinson previously analyzed cracks with nonplanar faces, and suggested that the crack face contact under combined loading conditions resulted in contact, friction, and even frictional locking.<sup>7</sup> While this explanation is feasible for many materials, this hypothesis predicts

that the pure mode II fracture toughness is higher than its mode I counterpart, which is not the case here. Also, during the experiment, the crack faces are separated (see *Figure 3*), so that crack face interaction does not explain the trend found here. Another near tip phenomenon, plasticity, has been postulated to explain differences in fracture toughness with mode mixity, but again higher mode II toughness is predicted.<sup>10</sup> More research needs to be done to explain the variations in fracture toughness and how this relates to the micromechanisms in the rubbery particulate composite.

Although the elliptical failure locus is an empirical curve fit and cannot now be linked to any explanations based on micromechanisms, the kink angles agreed approximately with several theoretical predictions. All of these theories differ only in the assumed determinant of initial crack growth direction. *Figure 6* shows the kink angles plotted against the crack orientation angle. The most closely agreeing theory is the strain energy density theory introduced in the 1970's by Sih and Chen.<sup>5,15</sup> The quantity that determines the initial crack trajectory is the strain energy density, which is a function of the two components of the complex stress intensity factor  $\bar{K}$  according to:

$$S = \alpha_{11}K_I^2 + 2\alpha_{12}K_IK_{II} + \alpha_{22}K_{II}^2 \quad (5)$$

The three coefficients  $\alpha_{11}$ ,  $\alpha_{12}$ , and  $\alpha_{22}$  depend on  $\theta$ , the material properties, and the stress state. The hypothesis is that the crack will grow at an angle such that the value of  $S$  will be maximized. Letting  $\partial S / \partial \theta$  equal zero and substituting for  $K_I$  and  $K_{II}$  from eqn (1) results in a prediction of the kink angle,  $\theta_0$ , for a simple plate geometry that relates to the crack orientation angle through:

$$(\kappa - 1)\sin(\theta_0 + 2\beta) - 2\sin(2\theta_0 + 2\beta) + \sin(2\theta_0) = 0 \quad (6)$$

Here  $\kappa = (3-4\nu)$  for plane stress and  $(3-\nu)/(1+\nu)$  for plane strain, where  $\nu$  is Poisson's ratio. Other theories worthy of mention are also shown in *Figure 6*; these are the maximum tangential stress and maximum energy release rate theories. The maximum tangential stress theory assumes that the crack grows so that  $\sigma_{\theta\theta}$  is maximized. The maximum energy release rate theory analyzes an imagined short extension of a main crack that grows from the

main crack at an angle,<sup>10</sup>. The local energy release rate for this crack can be expressed in terms of global factors ( $K_I$  and  $K_{II}$  for the larger crack), and the optimal orientation of this kinked crack will be that which maximizes the strain energy release rate,  $G$ .

One conclusion suggested by the *Figure 6* is that linear fracture mechanics theories can predict, with fair accuracy, the behavior of this rubbery particulate composite. This is true because the overall material response is linear for the conditions considered here. This is shown by the load displacement curves of the cracked specimens (see, for example, *Figure 7*). Another manifestation of the linear nature of the material response is shown in *Figure 8*.<sup>16</sup> This figure shows the measured and calculated crack opening displacements and also the measured and calculated  $v$  field fringe data for a moiré experiment performed on a similar material (for simplicity, mode I conditions are shown). The analysis used linear fracture mechanics concepts that are incorporated in the resulting calculated values shown in the figure. The close agreement between the experimental and the calculated fringe values and crack opening displacements suggests that the linear fracture mechanics assumptions are justified.

Linear fracture mechanics concepts also work well with growth rate predictions. *Figure 4* shows a growing mixed-mode crack modeled as an equivalent mode I crack. The crack growth rates, when determined in this way, can be plotted according to a power law:

$$\frac{da_{eff}}{dt} = CK_I^m \quad (7)$$

Here  $a_{eff}$  is the effective crack length and  $K_I$  is the mode I stress intensity factor; both are based on the model shown in *Figure 4b*. *Figure 9* shows the data for all the mixed-mode specimens plotted on a log-log graph of  $da_{eff}/dt$  versus  $K$ . The first few data points for each specimen have been deleted so that steady state conditions are achieved. The individual data sets all have about the same slope and can be assessed as an aggregate so that the parameters for the crack growth law (when analyzed using a least-squares technique) are found to be  $C = 1.79 \times 10^{-6}$  and  $m = 2.73$  for the material studied here (assuming  $da_{eff}/dt$  is in mm/s and  $K_I$  is in  $\text{kPa m}^{1/2}$ ). The pure mode I data gives comparable coefficients of  $C = 1.85 \times 10^{-6}$  and  $m = 2.74$ . We conclude that the more complicated geometry in *Figure 4a* can be analyzed using the simpler geometry of *Figure 4b* for the range of mixities tested.



## CONCLUSIONS

Although rubbery particulate composites have viscoelastic properties, high elongations, and complicated failure mechanisms, they can be studied, for a given nominal strain rate, using the principles of linear fracture mechanics. When analyzed in this way, the fracture locus is elliptical. The initial crack growth angles match the strain energy density theory best, although for all but the highest mode mixities, other theories gave nearly identical results. The crack growth rates can be predicted using a simplified mode I approach. These findings allow for a simplified approach that circumvents more elaborate and difficult analyses required by the consideration of nonlinear and time dependent effects. Future work could include the use of experimental methods to study the causes of fracture in these composites, especially the micromechanisms near the crack tip at various mode mixities.

## REFERENCES

- 1 Erdogan, F. and Sih, G. C. On the Crack Extension in Plates under Plane Loading and Transverse Shear. *J. Basic Engineering*, 1963, **85D**, 519-527.
- 2 Ravi-Chandar, K. and Liu, C. T., Mixed-Mode Fracture of Solid Propellants. *Society for Experimental Mechanics Spring Conference*, Dearborn, Michigan, June 7-9, 1993.
- 3 Ikeda, T., Miyazaki, N. and Soda, T. Mixed Mode Fracture Criterion of Interface Crack Between Dissimilar Materials. *Eng. Frac. Mech.*, 1998, **59**, 725-735.
- 4 Wu, E. M. Application of Fracture Mechanics to Anisotropic Plates. *J. Appl. Mech.*, 1967, **34**, 967-974.
- 5 Kanninen, M. F. and Popelar, C. H. *Advanced Fracture Mechanics*. Oxford University Press, New York, 1985.
- 6 Spencer, B. and Barnby, J. T. The Effects of Notch and Fibre Angles on Crack Propagation in Fibre-Reinforced Polymers. *Journal of Composite Materials*, 1976, **11**, 83-88.
- 7 Evans, A. G. and Hutchinson, J. W. Effects of Non-planarity on the Mixed Mode Fracture Resistance of Bimaterial Interfaces. *Acta Metallurgica*, 1989, **37**, 909-916.
- 8 Shih, C. F. and Suresh, S. Mixed-Mode Inelastic Crack-Tip Fields: Homogeneous Solids and Bimaterial Interfaces. *Scripta Metallurgica et Materialia*, 1991, **25**, 1017-1022.

- 9 Zafari, F., Ramulu, M. and Kobayashi, A. S., Mixed Mode Fracture in Thin Aluminum Sheets. *Abstract Proceedings of the Society for Experimental Mechanics Spring Conference*, Bellevue, Washington, June 2-4, 1997, pp. 74-75.
- 10 Hutchinson, J. W. and Suo, Z. Mixed Mode Cracking in Layered Materials. In *Advances in Applied Mechanics*, eds. J. W. Hutchinson and T. Y. Wu. Academic Press, New York, 1991, pp. 63-91.
- 11 Tvergaard, V. and Hutchinson, J. W. The Influence of Plasticity on Mixed Mode Interface Toughness. *J. Mech. Phys. Solids*, 1993, **41**, 1119-1135.
- 12 Anderson, T. L. *Fracture Mechanics: Fundamentals and Applications*, 1st edn. CRC Press, Boca Raton, FL, 1991.
- 13 Matos, P. P. L., McMeeking, R. M., Charalambides, P. G. and Drory, M. D. A Method for Calculating Stress Intensities in Bimaterial Fracture. *Int. J. Fracture*, 1989, **40**, 235-254.
- 14 Deming, W. E. *Statistical Adjustment of Data*. Dover Publications, New York, 1943.
- 15 Sih, G. C. and Chen, E. P. *Cracks in Composite Materials*. Martinus Nijhoff, The Hague, 1981.
- 16 Ravi-Chandar, K. Private communication, 1998.

## LIST OF FIGURES

Figure 1 - Schematic of a typical mixed-mode specimen (crack orientation is  $30^\circ$ )

Figure 2 - Sample finite element mesh for computational models (crack orientation is  $30^\circ$ )

Figure 3 - Crack in a specimen shortly after initiation of crack growth (crack orientation is  $60^\circ$ )

Figure 4 - Modeling mixed-mode crack growth using a simplified approach

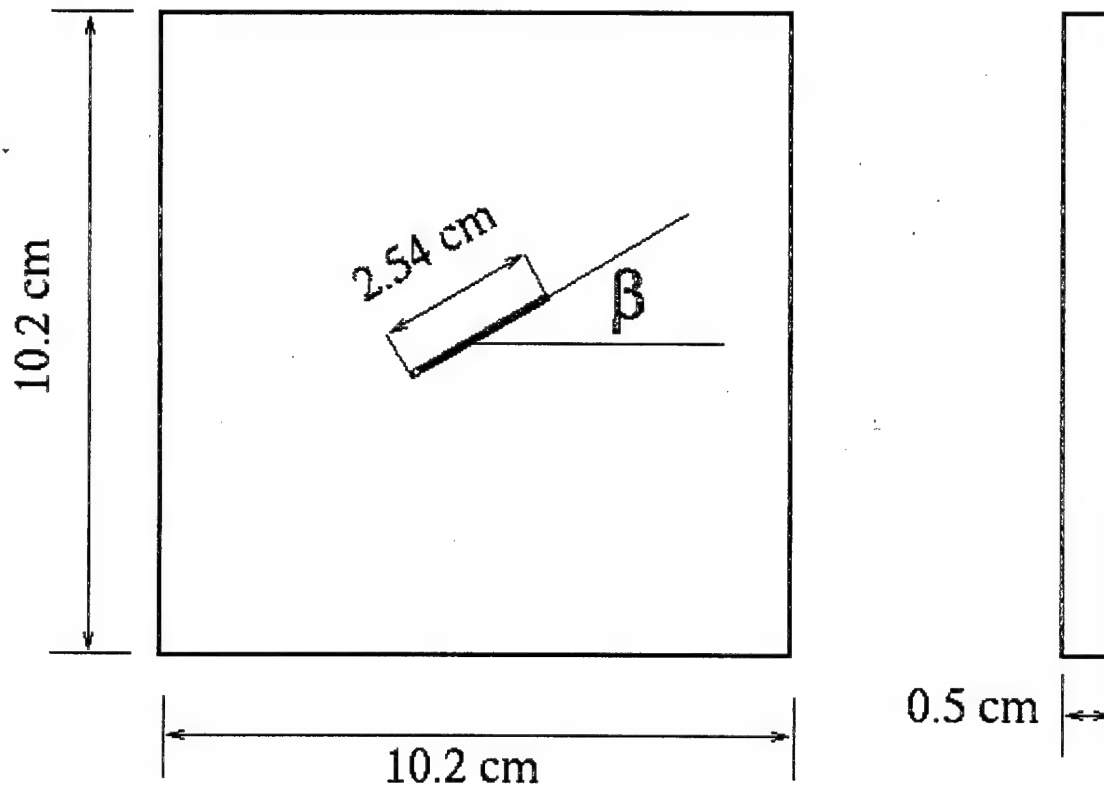
Figure 5 - Elliptical failure locus for initiation of crack growth

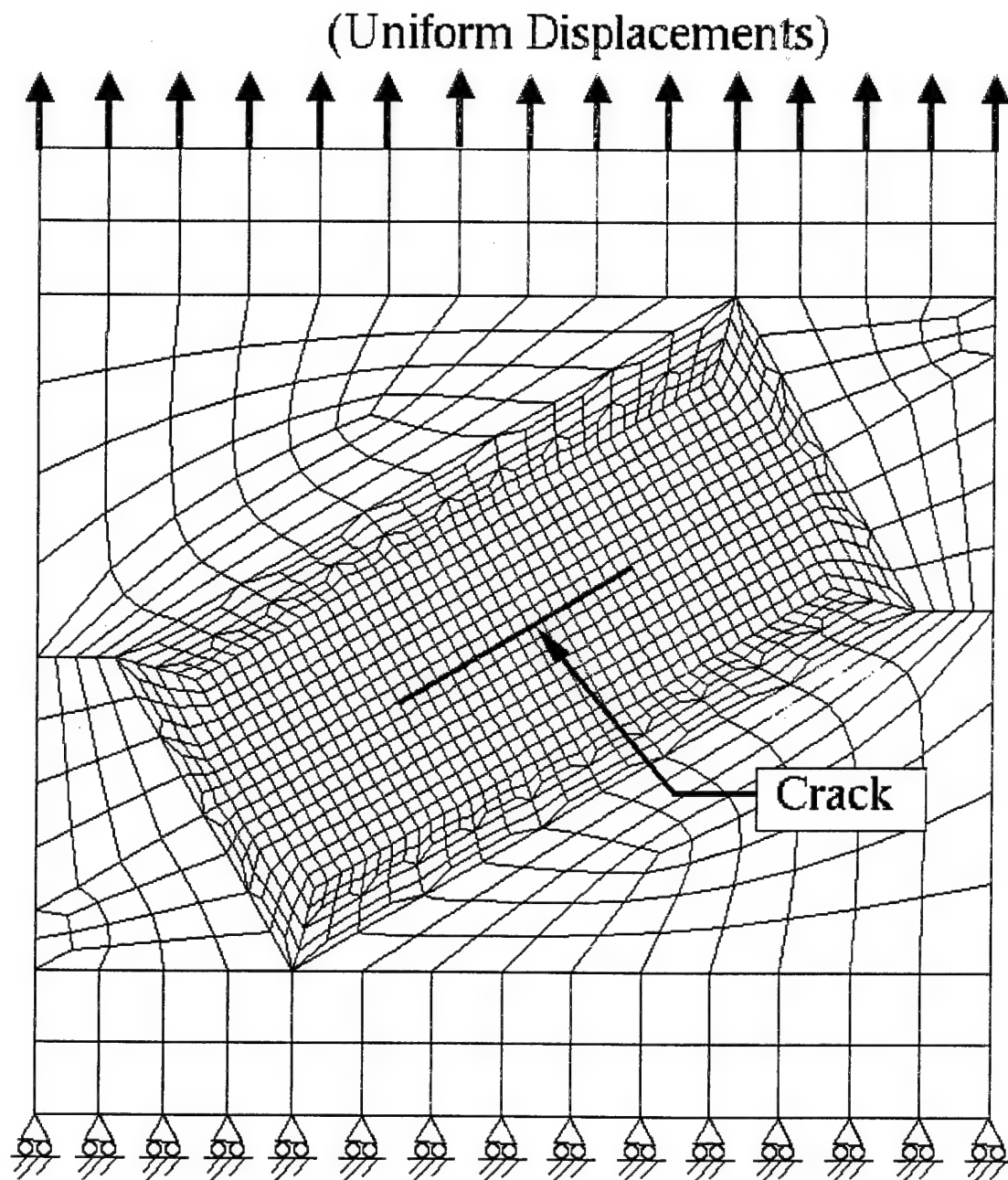
Figure 6 - Kink angles plotted as a function of crack orientation angle

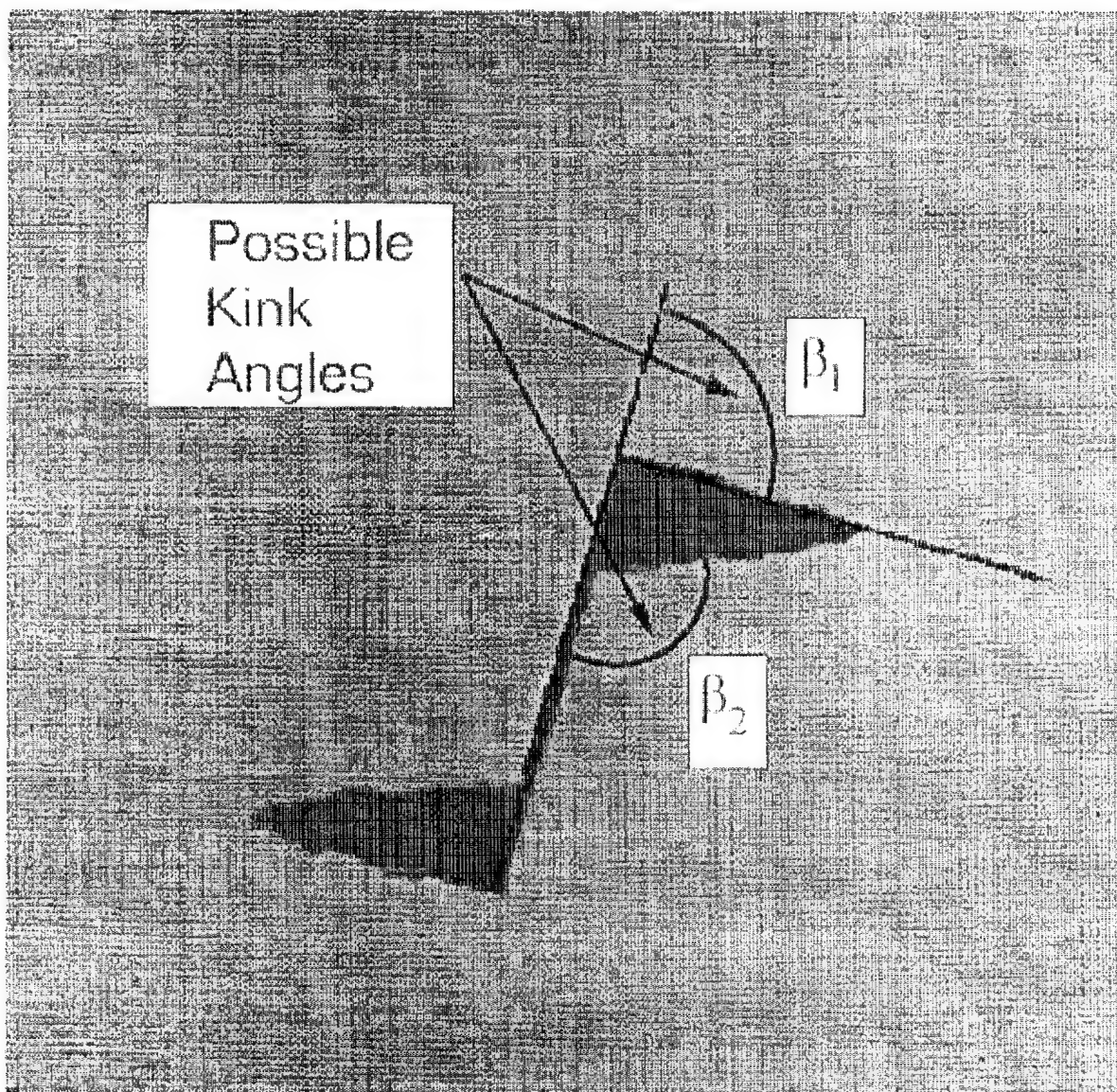
Figure 7 - Stress-strain curve and onset of crack growth for a typical specimen (crack orientation angle =  $30^\circ$ )

Figure 8 - Experimental and computed moiré fringes and crack opening displacement for a rubbery particulate composite

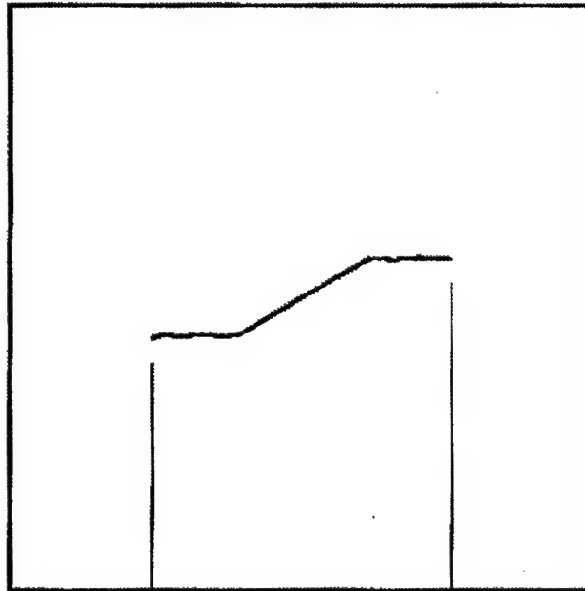
Figure 9 - Effective crack growth rate for the mixed-mode experiments as a function of stress intensity factor



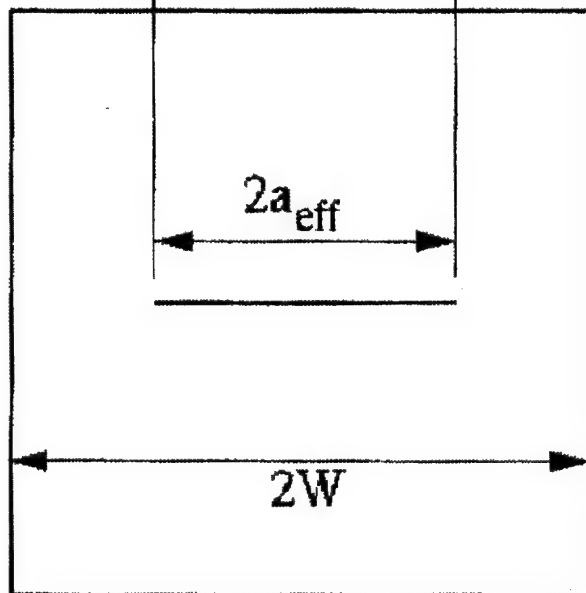


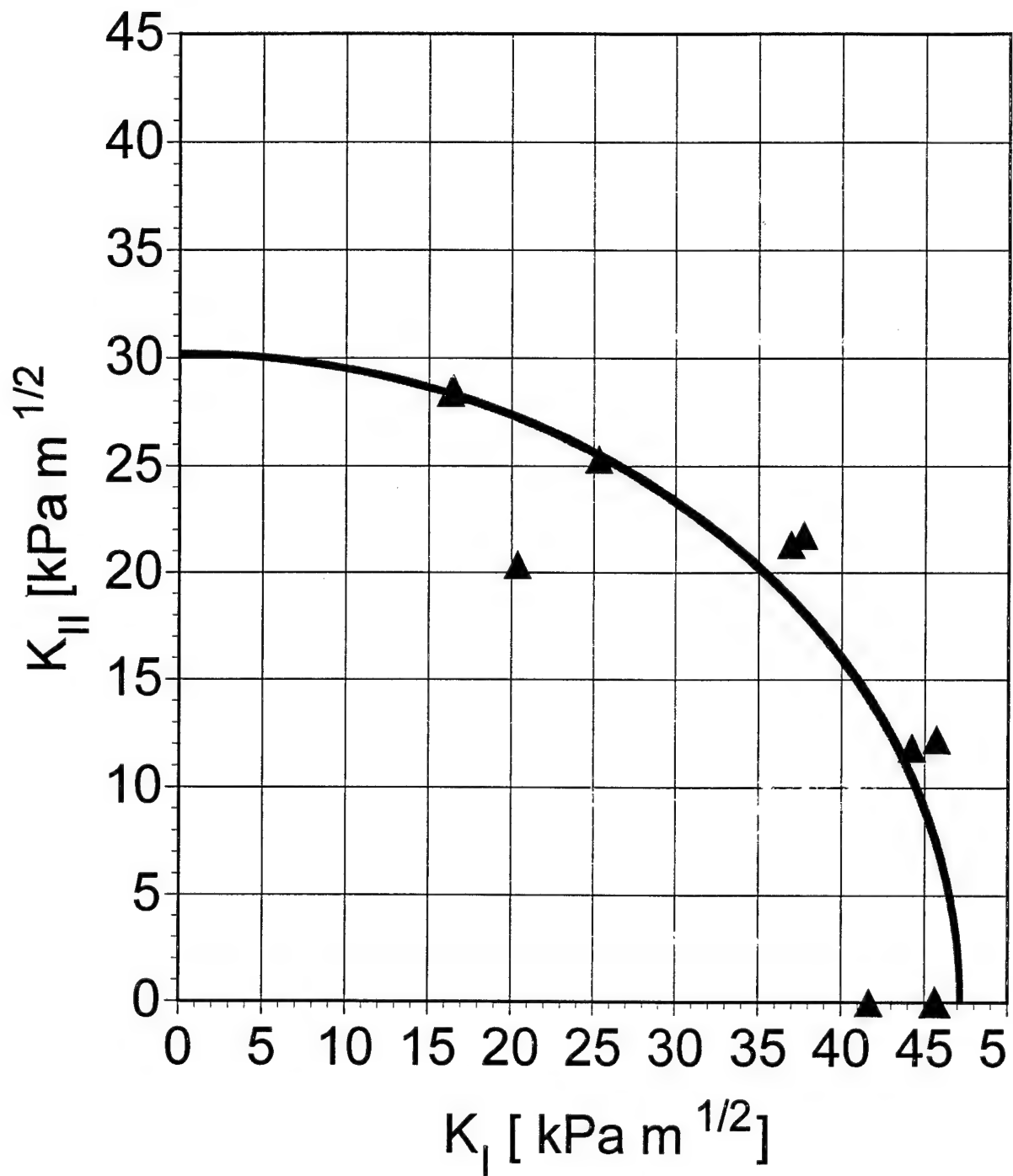


(a)

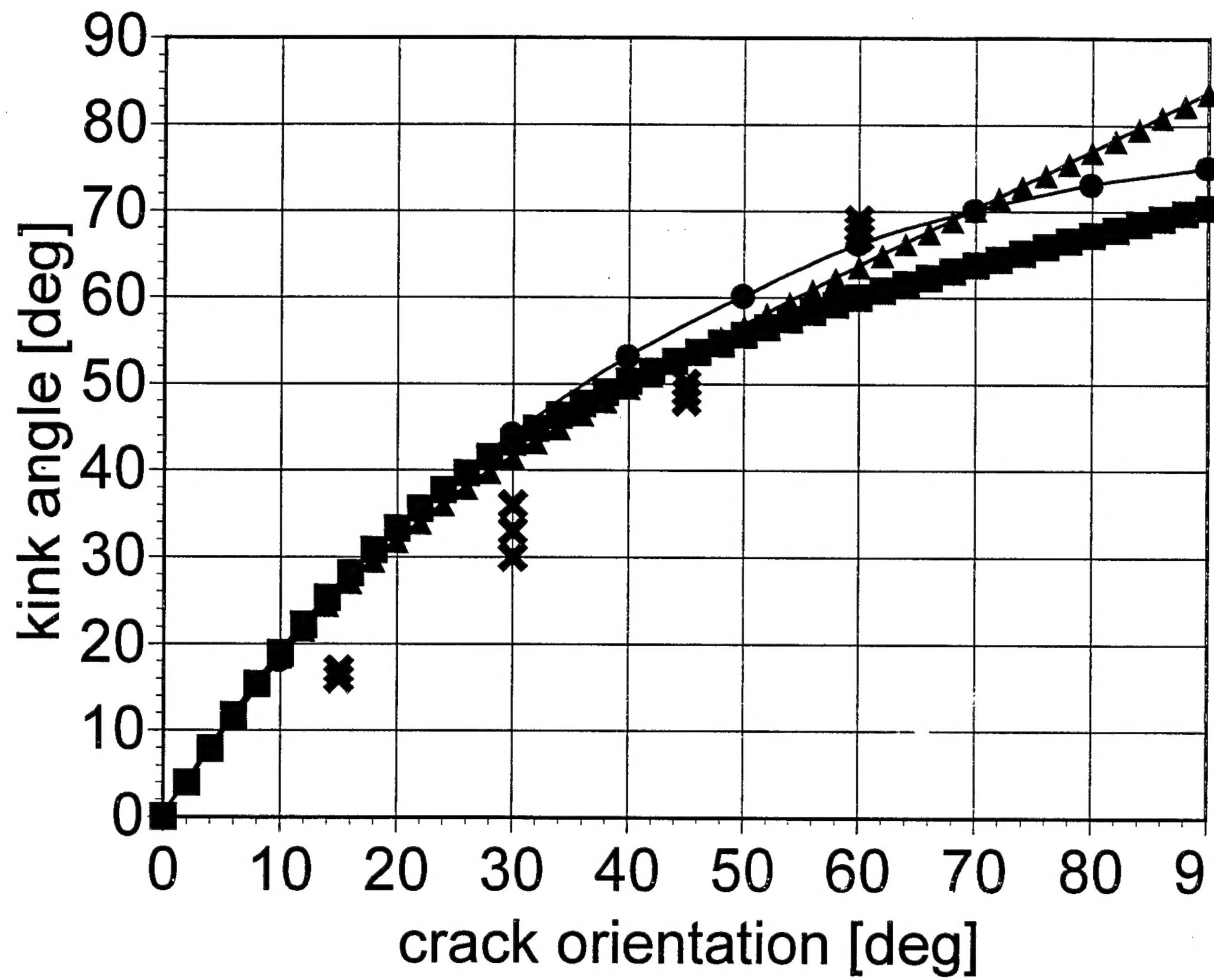


(b)









- max tensile stress
- max energy release rate
- ▲ max strain energy density
- × propellant experiments

